

Searching for the CEP location with nonlocal PNJL models constrained by Lattice QCD

Gustavo A. Contrera^{1,2,3 a}, A. Gabriela Grunfeld^{3,4} and David Blaschke^{5,6,7}

¹ IFLP, CONICET - Dpto. de Física, UNLP, La Plata, Argentina

² Gravitation, Astrophysics and Cosmology Group, FCAYG, UNLP, La Plata, Argentina

³ CONICET, Rivadavia 1917, 1033 Buenos Aires, Argentina

⁴ Departamento de Física, Comisión Nacional de Energía Atómica, (1429) Buenos Aires, Argentina

⁵ Institute for Theoretical Physics, University of Wrocław, 50-204 Wrocław, Poland

⁶ Joint Institute for Nuclear Research, 141980 Dubna, Moscow Region, Russia

⁷ National Research Nuclear University (MEPhI), 115409 Moscow, Russia

Received: date / Revised version: date

Abstract. We investigate the possible location of the critical end point in the QCD phase diagram based on nonlocal covariant PNJL models including a vector interaction channel. The form factors of the covariant interaction are constrained by lattice QCD data for the quark propagator. The comparison of our results for the pressure including the pion contribution and the scaled pressure shift $\Delta P/T^4$ vs T/T_c with lattice QCD results shows a better agreement when Lorentzian formfactors for the nonlocal interactions and the wave function renormalization are considered. The strength of the vector coupling is used as a free parameter which influences on results at finite baryochemical potential. It is used to adjust the slope of the pseudocritical temperature of the chiral phase transition at low baryochemical potential and the scaled pressure shift accessible in lattice QCD simulations. Our study supports the existence of a critical point and favors for its location the region $69.9 \text{ MeV} \leq T_{\text{CEP}} \leq 129.8 \text{ MeV}$ and $128.6 \text{ MeV} \leq \mu_{\text{CEP}} \leq 223.3 \text{ MeV}$ which is accessible in experiments at the NICA accelerator complex.

PACS. 05.70.Jk Critical point phenomena – 11.10.Wx Finite-temperature field theory – 11.30.Rd Chiral symmetries – 12.38.Mh Quark-gluon plasma – 25.75.Nq Quark deconfinement, quark-gluon plasma production, and phase transitions

The search for the location of the critical endpoint (CEP) of first order phase transitions in the QCD phase diagram is one of the objectives for beam energy scan (BES) programs in relativistic heavy-ion collision experiments at RHIC and SPS as well as in future ones at NICA and FAIR which try to identify the parameters of its position ($T_{\text{CEP}}, \mu_{\text{CEP}}$). From a theoretical point of view, the situation is very blurry since the predictions for this position form merely a skymap in the $T - \mu$ plane [1].

Lattice QCD results at zero and small chemical potential μ , show that the chiral and deconfinement transitions are crossover with a pseudocritical temperature of $T_c(0) = 154 \pm 9 \text{ MeV}$ [2].

However, at finite density lattice QCD suffers from the sign problem and only extrapolation or approximate techniques are available that work at finite quark densities. Therefore, nonperturbative methods and methods are inevitable tools in this region. As a consequence there is a variety of possibilities for the structure of the QCD phase

diagram and the position of the CEP. Let us mention few of them:

- no CEP at all [3], with crossover transition in the whole phase diagram,
- no CEP, but a Lifshitz point [4],
- one CEP, but with largely differing predictions of its position [1],
- second CEP [5, 6, 7],
- CEP and triple point, possibly coincident, considering another phase (i.e. color superconducting [8] or quarkyonic [9] matter) at low temperatures and high densities.

This situation is far from being satisfactory in view of the upcoming experimental programmes. An exhaustive analysis should be performed to predict a CEP region as narrow as possible, considering only those effective models that best reproduce recent lattice QCD results on the one hand and that obey constraints from heavy-ion collision experiments and compact star observations where available. In the present contribution, we discuss the existence and location of a CEP within the class of nonlocal

^a e-mail: contrera@fisica.unlp.edu.ar

chiral quark models coupled to the Polyakov loop potential, with vector channel interactions, on the selfconsistent meanfield level.

The Lagrangian of these models is given by

$$\mathcal{L} = \bar{q}(i\mathcal{D} - m_0)q + \mathcal{L}_{\text{int}} + \mathcal{U}(\Phi), \quad (1)$$

where q is the $N_f = 2$ fermion doublet $q \equiv (u, d)^T$, and m_0 is the current quark mass (we consider isospin symmetry, that is $m_0 = m_u = m_d$). The covariant derivative is defined as $D_\mu \equiv \partial_\mu - iA_\mu$, where A_μ are color gauge fields.

The nonlocal interaction channels are given in the current-current coupling form by

$$\mathcal{L}_{\text{int}} = -\frac{G_S}{2} [j_a(x)j_a(x) - j_P(x)j_P(x)] - \frac{G_V}{2} j_V(x)j_V(x),$$

(2) and Lorentzians with WFR

where the nonlocal generalizations of the currents are

$$\begin{aligned} j_a(x) &= \int d^4z g(z) \bar{q}\left(x + \frac{z}{2}\right) \Gamma_a q\left(x - \frac{z}{2}\right), \\ j_P(x) &= \int d^4z f(z) \bar{q}\left(x + \frac{z}{2}\right) \frac{i \overleftrightarrow{\not{D}}}{2\kappa_p} q\left(x - \frac{z}{2}\right), \\ j_V(x) &= \int d^4z g(z) \bar{q}\left(x + \frac{z}{2}\right) \gamma^0 q\left(x - \frac{z}{2}\right). \end{aligned} \quad (3)$$

with $\Gamma_a = (\Gamma_S, \Gamma_P) = (\mathbf{1}, i\gamma_5\boldsymbol{\tau})$ for scalar and pseudoscalar currents respectively, and $u(x') \overleftrightarrow{\not{D}} v(x) = u(x')\partial_x v(x) - \partial_x u(x')v(x)$. The functions $g(z)$ and $f(z)$ in Eq. (3) are nonlocal covariant form factors characterizing the corresponding interactions. The scalar-isoscalar component of the $j_a(x)$ current will generate the momentum dependent quark mass in the quark propagator, while the ‘‘momentum’’ current, $j_P(x)$, will be responsible for a momentum dependent wave function renormalization (WFR) of this propagator. Note that the relative strength between both interaction terms is controlled by the mass parameter κ_p introduced in Eq. (3). Finally, $j_V(x)$ represents the vector channel interaction current, whose coupling constant G_V is usually taken as a free parameter.

In what follows it is convenient to Fourier transform into momentum space. Since we are interested in studying the characteristics of the chiral phase transition we have to extend the effective action to finite temperature T and chemical potential μ . In the present work this is done by using the Matsubara imaginary time formalism. Concerning the gluon degrees of freedom we employ the Polyakov-loop extension of nonlocal chiral quark models according to prescriptions described in previous works [10, 11, 12, 13, 14]. In the present work we have chosen a μ -dependent logarithmic effective potential described in [15].

$$\mathcal{U}(\Phi, T, \mu) = (a_0 T^4 + a_1 \mu^4 + a_2 T^2 \mu^2) \Phi^2 + a_3 T_0^4 \ln(1 - 6\Phi^2 + 8\Phi^3 - 3\Phi^4), \quad (4)$$

where there parameters are $a_0 = -1.85$, $a_1 = -1.44 \times 10^{-3}$, $a_2 = -0.08$, $a_3 = -0.40$. For the T_0 parameter we use the

value corresponding to two flavors $T_0 = 208$ MeV, as it has been suggested in Ref. [16] and already employed in nonlocal PNJL models in [12, 17].

Finally, in order to fully specify the nonlocal model under consideration we set the model parameters as well as the form factors $g(q)$ and $f(q)$ following Refs. [11], [18] and [19], i.e. considering two different types of functional dependencies for these form factors: exponential forms

$$\text{(Set A)} \quad \begin{cases} g(p) = \exp(-p^2/\Lambda_0^2) \\ f(p) = 0 \end{cases}, \quad (5)$$

$$\text{(Set B)} \quad \begin{cases} g(p) = \exp(-p^2/\Lambda_0^2) \\ f(p) = \exp(-p^2/\Lambda_1^2) \end{cases}, \quad (6)$$

$$\text{(Set C)} \quad \begin{cases} g(p) = \frac{1+\alpha_z}{1+\alpha_z f_z(p)} \frac{\alpha_m f_m(p) - m}{\alpha_m - m} \frac{\alpha_z f_z(p)}{\alpha_z} \\ f(p) = \frac{1+\alpha_z}{1+\alpha_z f_z(p)} f_z(p) \end{cases}, \quad (7)$$

where

$$\begin{aligned} f_m(p) &= [1 + (p^2/\Lambda_0^2)^{3/2}]^{-1}, \\ f_z(p) &= [1 + (p^2/\Lambda_1^2)]^{-5/2}, \end{aligned} \quad (8)$$

and $\alpha_m = 309$ MeV, $\alpha_z = -0.3$. Further details on the parameters can be found in Ref. [19] and the reference quoted therein.

Within this framework the thermodynamic potential in the mean field approximation (MFA) reads

$$\begin{aligned} \Omega^{\text{MFA}} &= -4T \sum_c \sum_n \int \frac{d^3\mathbf{p}}{(2\pi)^3} \ln \left[\frac{(\tilde{\rho}_{n,\mathbf{p}}^c)^2 + M^2(\rho_{n,\mathbf{p}}^c)}{Z^2(\rho_{n,\mathbf{p}}^c)} \right] \\ &+ \frac{\sigma_1^2 + \kappa_p^2 \sigma_2^2}{2G_S} - \frac{\omega^2}{2G_V} + \mathcal{U}(\Phi, T). \end{aligned} \quad (9)$$

where $M(p)$ and $Z(p)$ are given by

$$\begin{aligned} M(p) &= Z(p) [m + \sigma_1 g(p)], \\ Z(p) &= [1 - \sigma_2 f(p)]^{-1}. \end{aligned} \quad (10)$$

In addition, we have defined [20]

$$(\rho_{n,\mathbf{p}}^c)^2 = [(2n+1)\pi T - i\mu + \phi_c]^2 + \mathbf{p}^2, \quad (11)$$

where the quantities ϕ_c are given by the relation $\phi = \text{diag}(\phi_r, \phi_g, \phi_b)$. Namely, $\phi_c = c \phi_3$ with $c = 1, -1, 0$ for r, g, b , respectively.

In the case of $(\tilde{\rho}_{n,\mathbf{p}}^c)$ we have used the same definition as in Eq.(11) but shifting the chemical potential according to [19]

$$\tilde{\mu} = \mu - \omega g(p) Z(p). \quad (12)$$

We also want to include in our analysis the results arising from a local PNJL model based on [21] with two

flavors instead of three. Moreover, we consider that the chemical potential is shifted by

$$\tilde{\mu} = \mu - \omega. \quad (13)$$

Ω^{MFA} turns out to be divergent and, thus, needs to be regularized. For this purpose we use the same prescription as in Refs. [22, 11]. The mean field values $\sigma_{1,2}$, ω and ϕ_3 at a given temperature or chemical potential, are obtained from a set of four coupled ‘‘gap’’ equations which come from the minimization of the regularized thermodynamic potential, that is

$$\frac{\partial \Omega_{\text{reg}}^{\text{MFA}}}{\partial \sigma_1} = \frac{\partial \Omega_{\text{reg}}^{\text{MFA}}}{\partial \sigma_2} = \frac{\partial \Omega_{\text{reg}}^{\text{MFA}}}{\partial \omega} = \frac{\partial \Omega_{\text{reg}}^{\text{MFA}}}{\partial \phi_3} = 0. \quad (14)$$

As a starting point we choose a step function for the form-factor, using in this case the parameters in [23]. This resembles the local limit of the present model and results can be compared, e.g., with Refs. [3] and [24]. As in our previous work [19], the model inputs have been constrained with results from lattice QCD studies. In particular, the form factors of the nonlocal interaction can be chosen such as to reproduce the dynamical mass function $M(p)$ and the WFR function $Z(p)$ of the quark propagator in the vacuum [25]. In Fig. 1 we show the shapes of normalized masses and WFR for the models under discussion here, i.e., the nonlocal models of Set A (rank-one), Set B and Set C (rank-two) as well as the local limit. From this figure we see that Set C fits best the normalized dynamical mass.

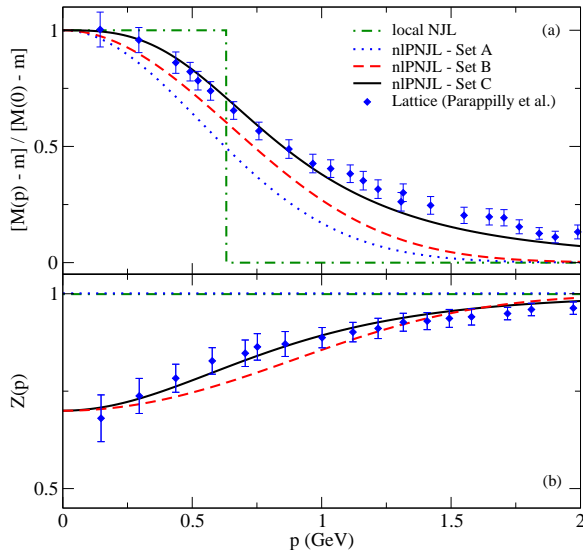


Fig. 1. (Adapted from Ref. [18]). Normalized dynamical masses for the different form factors under study and wave function renormalization for Set B and Set C, fitted to lattice QCD data [25].

Now we are in the position to discuss the results for the thermodynamics of the nonlocal PNJL models, starting

from the pressure $P(\mu, T) = -\Omega_{\text{reg}}^{\text{MFA}}$. In the upper panel of Fig. 2 we compare the pressure shift $\Delta P = P(\mu, T) - P(0, T)$ scaled with T^4 as function of T/T_c for all sets of parametrizations shown in Fig. 1 to lattice results from [26, 27]. It is obvious that the best obtained fit corresponds to Set C, supporting the robustness of rank-2 Lorentzian parametrization. In the lower panel of Fig. 2 we show a comparison between Set C and lattice results [26].

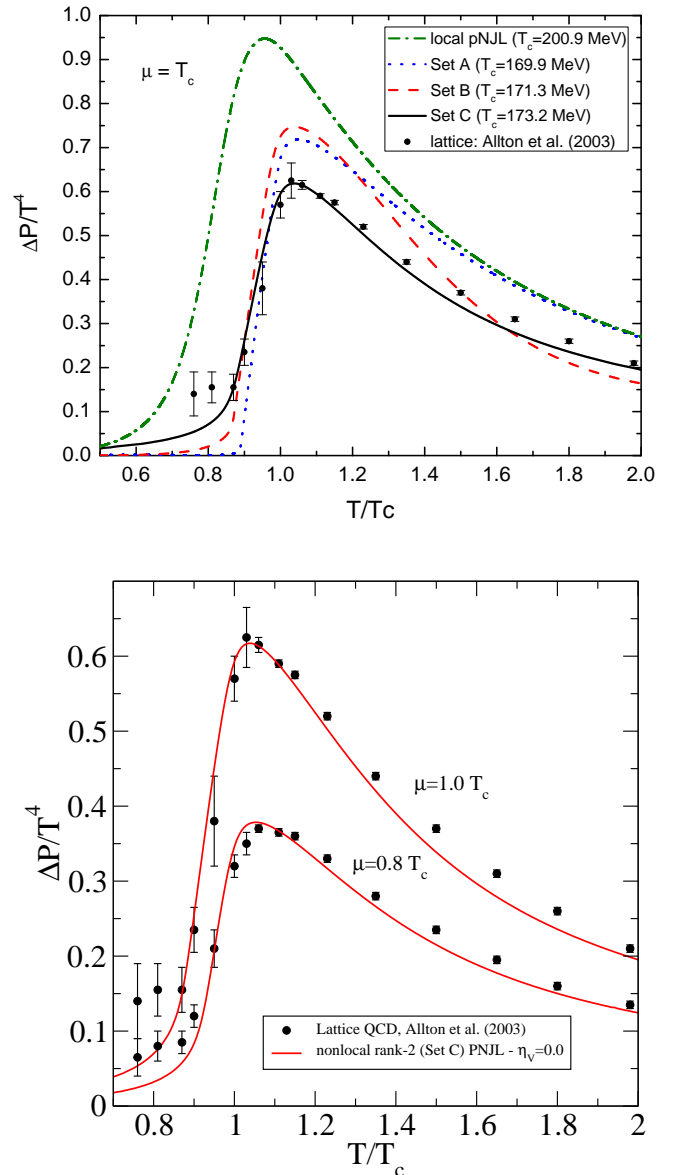


Fig. 2. The scaled pressure shift $\Delta P/T^4$ as a function of the scaled temperature T/T_c . Upper panel: Comparison of the lattice QCD data [26] with results of local and nonlocal pNJL models. Lower panel: Comparison of Set C results with lattice QCD [26] for two chemical potentials $\mu = 1.0 T_c$ and $\mu = 0.8 T_c$.

In Fig. 3 we show a comparison of the pressure normalized to the Stefan-Boltzmann limit (P_{SB}) to lattice QCD results from [28]. In this figure it can be seen that the pion pressure dominates the pressure dependence for $T < T_c$ and quickly vanishes for $T > T_c$ as a result of the Mott dissociation of the pion.

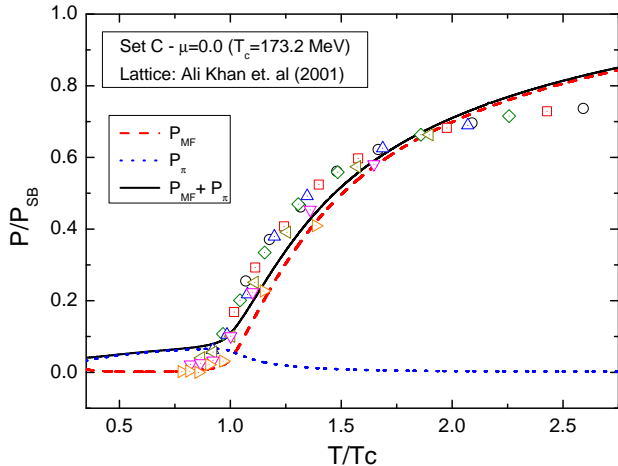


Fig. 3. Comparison of the pressure in units of its Stefan-Boltzmann value between Set C (with and without pion pressure) and lattice QCD results [28] as function of T/T_c .

From the above results, Set C appears to be the appropriate choice to best fit lattice QCD results.

As mentioned above, the vector coupling G_V is considered a free parameter. In Fig. 4 we show again $\Delta P/T^4$ vs. T/T_c as in Fig. 3 but now considering different vector coupling parameters $\eta_V = G_V/G_S$ just for Set C. The best agreement with lattice QCD data is obtained for $\eta_V = 0$, i.e. for deactivated vector channel. The consequences will be discussed below.

In MFA the vector coupling channel has a direct influence on the μ -dependence of the pseudocritical temperature $T_c(\mu)$ in the QCD phase diagram. In lattice QCD this dependence has been analyzed by Taylor expansion techniques [29] as

$$T_c(\mu)/T_c(0) = 1 - \kappa(\mu/T)^2 + \mathcal{O}[(\mu/T)^4], \quad (15)$$

with $\kappa = 0.059(2)(4)$ being the curvature. We will refer to this situation as LR I (lattice results I). In the same way, the vector coupling channel can be tuned to reproduce the curvature given by recent lattice QCD results based on imaginary chemical potential technique which gives $\kappa = 0.1341 \pm 0.019$ [30] and $\kappa = 0.1215 \pm 0.018$ [31], we call it LR II.

The curvatures can be determined from the phase diagrams. To do so, we plotted the pseudocritical temperatures of the crossover transitions as function of $(\mu/T)^2$ for different values of the vector coupling parameter η_V . Then, the curvatures can be obtained from the slope of the straight lines in the region of low (μ/T) values.

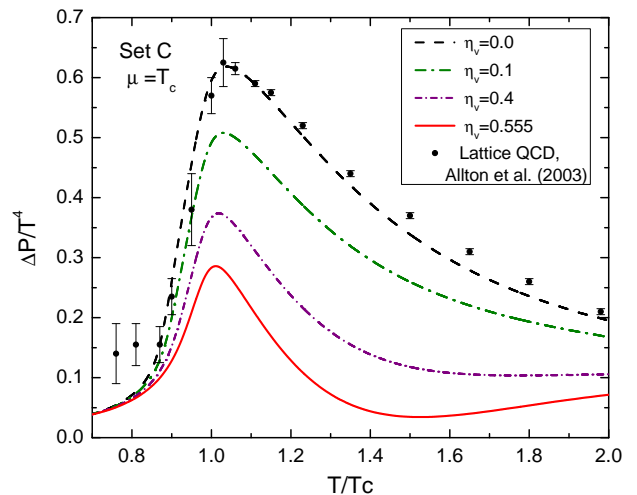


Fig. 4. Comparison between Set C results for different values of the vector coupling parameter η_V and lattice QCD data [26].

An example of this is shown in Figure 5 for set C (the corresponding plots for the other sets are qualitatively very similar). The fit (15) of the lattice QCD results, LR I, is also shown. The grey zone corresponds to the error in the coefficient κ obtained in [29].

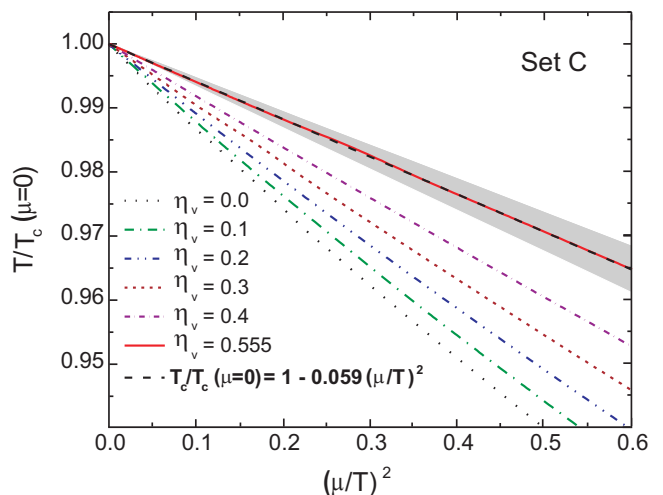


Fig. 5. (Color online) Chiral crossover transitions at low values of μ/T for different values of the vector coupling ratios $\eta_V = G_V/G_S$ for Set C. The dashed line corresponds to the lattice QCD prediction of $\kappa = 0.059(2)(4)$, LR I, [29].

In Fig. 6 we compare the lattice QCD results for both, LR I and LR II, with the values for the coefficient κ obtained within all PNJL models under study, considering different values of η_V .

Note that for fitting the lattice QCD value in the local model a larger vector coupling is required than in the nonlocal ones. Also the absolute value of the critical tem-

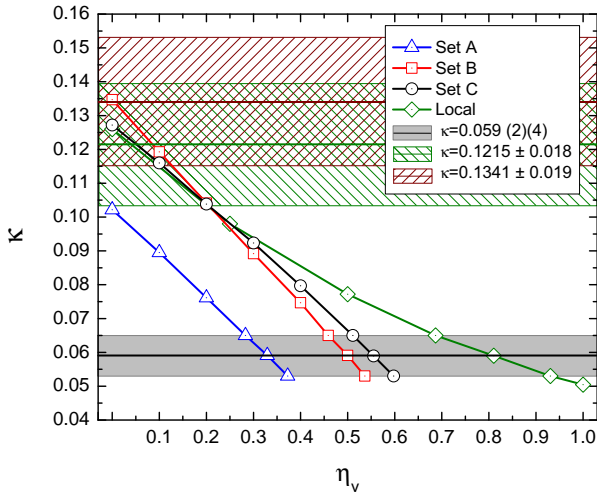


Fig. 6. (Color online) Curvature κ of the pseudocritical temperature $T_c(\mu)$ of the chiral crossover transition at low values of μ/T . The black line corresponds to the lattice QCD prediction of $\kappa = 0.059(2)(4)$ [29], while the brown (green) lines with hatched error regions come from analyses within the imaginary chemical potential method, resulting in $\kappa = 0.1341 \pm 0.019$ [30] ($\kappa = 0.1215 \pm 0.018$ [31]).

perature $T_c(0)$ in the local model is significantly different (larger) than in the nonlocal one.

The phase diagram with (pseudo-)critical temperatures $T_c(\mu)$ and critical points for Set C, i.e. the parametrization that best fits lattice QCD results (see Figs. 1 to 3) are shown in Fig. 7. The finite vector coupling parameter η_V is chosen to reproduce the curvature value for LR I at low μ . We found that switching off the vector interaction can reproduce both, the curvature obtained in LR II and the $\Delta P/T^4$ vs. T/T_c from Fig. 2¹.

Now we also considered the pseudo-critical deconfinement lines for $\Phi = 0.4 - 0.6$ in Fig. 7. As expected, the influence of vector interaction becomes stronger for higher densities (i.e. higher μ values).

The values for $T_c(\mu = 0)$ (in MeV) are 169.9, 171.3, 173.2 and 200.9, for Sets A, B, C and local, respectively. These results indicate that the $T_c(0)$ of nonlocal covariant PNJL models is rather insensitive to the choice of the form factors parametrizing the momentum dependence (running) of the dynamical mass function and the WFR function of the quark propagator as measured on the lattice at zero temperature [25], whereas the position of the CEP and critical chemical potential at $T = 0$ strongly depends on it.

In view of this finding, the absence of a CEP reported in the local limit [3] as well as the result for Set A without WFR seems to be less realistic (see Ref.[19]).

¹ Note that in Refs. [30,31] the values are quoted in the $T - \mu_B^2$ plane, while we are addressing the quark chemical potential instead of the baryon one. So the difference in the κ coefficients is a factor 9.

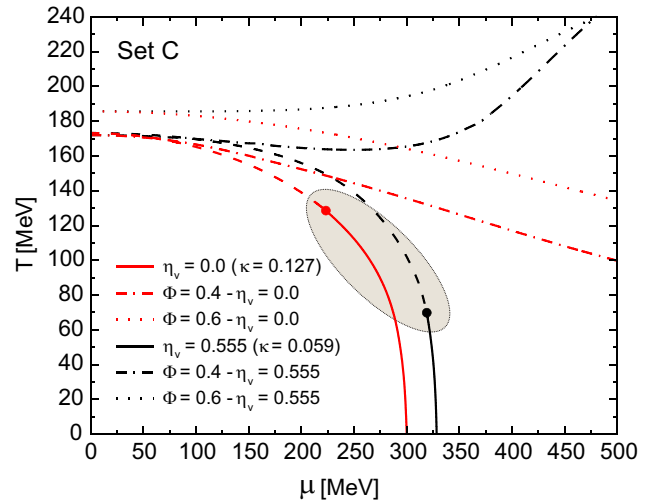


Fig. 7. Phase diagrams with (pseudo)critical temperatures $T_c(\mu)$ and critical points for nonlocal rank-2 PNJL model (Set C). Dashed (full) lines correspond to crossover (first order) transitions. The corresponding dash-dotted and dotted lines represent the deconfinement transition range, i.e. $\Phi = 0.4$ and $\Phi = 0.6$, resp. The highlighted region denotes the CEP position favored by the present study.

On the other hand, more recent lattice results [30,31] (LR II) suggest higher values for the κ coefficient, what implies a lower or even vanishing vector coupling parameter η_V , giving better agreement for $\Delta P/T^4$ vs. T/T_c .

Considering the different lattice constraints for κ and that the best fitting rank-2 nonlocal PNJL model is the one with Lorentzian form factors (Set C parametrization), the region in the QCD phase diagram where the CEP should be located according to our study, would be determined as $(T_{\text{CEP}}, \mu_{\text{CEP}}) = (128.6 \text{ MeV}, 223.3 \text{ MeV})$ for $\eta_V = 0.0$ and $(T_{\text{CEP}}, \mu_{\text{CEP}}) = (69.9 \text{ MeV}, 319.1 \text{ MeV})$ for $\eta_V = 0.555$. This region is highlighted in Fig. 7.

With this result of the present study we arrive at our conclusion for the NICA experiments which are devoted to the study of the quark-hadron mixed phase that shall be located at $T < T_{\text{CEP}}$ and $\mu > \mu_{\text{CEP}}$. We shall estimate whether the planned energy ranges of the BM@N experiment ($E_{\text{lab}} = 2 - 4 \text{ A GeV}$) and of the MPD experiment ($\sqrt{s_{NN}} = 4 - 11 \text{ GeV}$) are suitable for accessing the region of the mixed phase that follows from our study. To this end we use a parametrization for the chemical freeze-out temperature in the QCD phase diagram by Andronic *et al.* [32]

$$T_{\text{freeze}} = T_{\text{lim}} \left(1 - \frac{1}{0.7 + [\exp(\sqrt{s_{NN}}(\text{GeV})) - 2.9]/1.5} \right) \quad (16)$$

as obtained from statistical model analyses of hadron production in heavy-ion collision experiments, with $T_{\text{lim}} = 161 \pm 4 \text{ MeV}$. According to this parametrization and to the LR-I motivated nonlocal PNJL model with vanishing vector coupling, one should expect signals of a first order phase transition in collisions with $\sqrt{s_{NN}} \lesssim 6 \text{ GeV}$, right in the middle of the MPD energy scan. For the LR-II mo-

tivated parametrization with $\eta_V = 0.555$ the CEP is at such a low temperature that only the BM@N experiment has a chance to access the mixed phase, at laboratory energies $E_{\text{lab}} \lesssim 3$ A GeV, within the range of this fixed target experiment but too low for the collider experiment MPD.

The main conclusion of this study is that for the search of CEP signatures and the investigation of properties of the quark-hadron mixed phase in BES programmes the energy range of the NICA and FAIR facilities shall be particularly promising. We find a certain preference for a CEP position at a critical temperature $T_{\text{CEP}} \sim 130$ MeV, expected to be crossed in collisions with $\sqrt{s_{NN}} \sim 6$ GeV, corresponding to $E_{\text{lab}} \sim 18$ A GeV. This energy could not be reached from above by the present RHIC BES programme of the STAR experiment (lower limit $\sqrt{s_{NN}} = 7.7$ GeV and also not in the NA49 experiment at CERN SPS (lower limit $E_{\text{lab}} = 20$ A GeV). Just the ongoing NA61-SHINE experiment has a lower limit of $E_{\text{lab}} = 13$ A GeV in their energy scan that would allow to cross this suspected critical point (unless it would be located at slightly lower temperature). The old AGS experiment at BNL did not quite reach this energy (maximum energy $E_{\text{lab}} = 10.74$ A GeV) and were also not designed for a CEP search, while the energies at the GSI SIS are probably too low to reach the phase transition border (maximum energy $E_{\text{lab}} = 2$ A GeV). The theoretical investigation of the baryon stopping as a probe of the onset of deconfinement in heavy-ion collisions [33] have revealed a characteristic "wobble" structure in the curvature of the proton rapidity distribution at $\sqrt{s_{NN}} \sim 6$ GeV which remains robust also when applying acceptance cuts of the MPD experiment [34] at NICA. The MPD experiment at NICA will be the first dedicated heavy-ion collision experiment of the third generation to fully cover the suspected location of the CEP and thus to enter the mixed phase region via a first order phase transition. Contrary to studies with the local NJL model which first in [35] and more recently in [3] have shown that a CEP may be absent at all in the phase diagram for finite coupling in the repulsive vector channel, the present work with nonlocal PNJL models constrained by lattice QCD propagator data has shown that the presence of a CEP in the QCD phase diagram is rather robust against even stronger vector channel interactions.

Finally, we like to mention currently ongoing developments of our approach to the QCD phase diagram and the EoS of matter under extreme conditions:

- extension of the model to 2+1 flavours in order to properly compare with modern lattice QCD results [36, 37].
- investigate the robustness of the results of the non-local PNJL models when modifying the choice of the Polyakov-loop potential taking into account recent developments [38, 39, 40].
- add quark pair interaction channels and the possibility of color superconducting quark matter phases [23, 41]
- go beyond the mean field approximation within a Beth-Uhlenbeck approach [42].

A key quantity for such studies are the hadronic phase shifts. First results using a generic ansatz [43] for joining the hadron resonance gas and PNJL approaches are promising [44].

Acknowledgement

We would like to thank to O. Kaczmarek for useful comments and discussions. D.B. acknowledges hospitality and support during his visit at University of Bielefeld and funding of his research provided by the Polish NCN within the "Maestro" grant programme, under contract number UMO-2011/02/A/ST2/00306. G.C. and A.G.G. acknowledge financial support of CONICET and UNLP (Argentina).

References

1. M. A. Stephanov, PoS LAT **2006**, 024 (2006).
2. A. Bazavov, T. Bhattacharya, M. Cheng, C. DeTar, H. T. Ding, S. Gottlieb, R. Gupta and P. Hegde *et al.*, Phys. Rev. D **85**, 054503 (2012).
3. N. M. Bratovic, T. Hatsuda and W. Weise, Phys. Lett. B **719**, 131 (2013).
4. S. Carignano, D. Nickel, and M. Buballa, Phys. Rev. D **82**, 054009 (2010).
5. M. Kitazawa, T. Koide, T. Kunihiro and Y. Nemoto, Prog. Theor. Phys. **108**, 929 (2002).
6. D. Blaschke, M. K. Volkov and V. L. Yudin, Eur. Phys. J. A **17**, 103 (2003).
7. T. Hatsuda, M. Tachibana, N. Yamamoto and G. Baym, Phys. Rev. Lett. **97**, 122001 (2006).
8. D. Blaschke, H. Grigorian, A. Khalatyan and D. N. Voskresensky, Nucl. Phys. Proc. Suppl. **141**, 137 (2005).
9. A. Andronic, D. Blaschke, P. Braun-Munzinger, J. Cleymans, K. Fukushima, L. D. McLerran, H. Oeschler and R. D. Pisarski *et al.*, Nucl. Phys. A **837**, 65 (2010).
10. G. A. Contrera, D. Gomez Dumm and N. N. Scoccola, Phys. Lett. B **661** (2008) 113.
11. G. A. Contrera, M. Orsaria and N. N. Scoccola, Phys. Rev. D **82**, 054026 (2010).
12. D. Horvatic, D. Blaschke, D. Klabucar, O. Kaczmarek, Phys. Rev. D **84**, 016005 (2011).
13. A. E. Radzhabov, D. Blaschke, M. Buballa and M. K. Volkov, Phys. Rev. D **83**, 116004 (2011).
14. S. Benic, D. Blaschke, G. A. Contrera and D. Horvatic, Phys. Rev. D **89**, no. 1, 016007 (2014).
15. V. A. Dexheimer and S. Schramm, Phys. Rev. C **81**, 045201 (2010).
16. B. -J. Schaefer, J. M. Pawłowski and J. Wambach, Phys. Rev. D **76**, 074023 (2007).
17. V. Pagura, D. Gómez Dumm and N. N. Scoccola, Phys. Lett. B **707**, 76 (2012).
18. S. Noguera and N. N. Scoccola, Phys. Rev. D **78**, 114002 (2008).
19. G. A. Contrera, A. G. Grunfeld and D. B. Blaschke, Phys. Part. Nucl. Lett. **11**, 342 (2014).
20. D. B. Blaschke, D. Gomez Dumm, A. G. Grunfeld, T. Klähn and N. N. Scoccola, Phys. Rev. C **75**, 065804 (2007).

21. K. Fukushima, Phys. Rev. D **77**, 114028 (2008).
22. D. Gomez Dumm and N. N. Scoccola, Phys. Rev. C **72**, 014909 (2005).
23. D. Gomez Dumm, D. B. Blaschke, A. G. Grunfeld and N. N. Scoccola, Phys. Rev. D **78**, 114021 (2008).
24. A. V. Friesen, Y. L. Kalinovsky and V. D. Toneev, Int. J. Mod. Phys. A **30**, no. 16, 1550089 (2015).
25. M. B. Parappilly, P. O. Bowman, U. M. Heller, D. B. Leinweber, A. G. Williams and J. B. Zhang, Phys. Rev. D **73**, 054504 (2006).
26. C. R. Allton, S. Ejiri, S. J. Hands, O. Kaczmarek, F. Karsch, E. Laermann and C. Schmidt, Phys. Rev. D **68**, 014507 (2003).
27. Z. Fodor, S. D. Katz and K. K. Szabo, Phys. Lett. B **568**, 73 (2003).
28. A. Ali Khan *et al.* [CP-PACS Collaboration], Phys. Rev. D **64**, 074510 (2001).
29. O. Kaczmarek, F. Karsch, E. Laermann, C. Miao, S. Mukherjee, P. Petreczky, C. Schmidt, W. Soeldner and W. Unger, Phys. Rev. D **83**, 014504 (2011).
30. R. Bellwied, S. Borsanyi, Z. Fodor, J. Gnther, S. D. Katz, C. Ratti and K. K. Szabo, arXiv:1507.07510 [hep-lat].
31. C. Bonati, M. DElia, M. Mariti, M. Mesiti, F. Negro and F. Sanfilippo, Phys. Rev. D **92**, no. 5, 054503 (2015)
32. A. Andronic, P. Braun-Munzinger and J. Stachel, Nucl. Phys. A **772**, 167 (2006).
33. Y. B. Ivanov, Phys. Lett. B **721**, 123 (2013).
34. Y. B. Ivanov and D. Blaschke, Phys. Rev. C **92**, no. 2, 024916 (2015).
35. C. Sasaki, B. Friman and K. Redlich, Phys. Rev. D **75**, 054026 (2007)
36. S. Borsanyi, Z. Fodor, C. Hoelbling, S. D. Katz, S. Krieg and K. K. Szabo, Phys. Lett. B **730**, 99 (2014).
37. A. Bazavov *et al.* [HotQCD Collaboration], Phys. Rev. D **90**, 094503 (2014).
38. C. Sasaki and K. Redlich, Phys. Rev. D **86**, 014007 (2012).
39. M. Ruggieri, P. Alba, P. Castorina, S. Plumari, C. Ratti and V. Greco, Phys. Rev. D **86**, 054007 (2012).
40. K. Fukushima and K. Kashiwa, Phys.Lett. B **723**, 360 (2013).
41. D. B. Blaschke, F. Sandin, V. V. Skokov and S. Typel, Acta Phys. Polon. Supp. **3**, 741 (2010).
42. D. Blaschke, M. Buballa, A. Dubinin, G. Roepke and D. Zablocki, Annals Phys. **348**, 228 (2014).
43. D. Blaschke, A. Dubinin and L. Turko, Phys. Part. Nucl. **46**, no. 5, 732 (2015).
44. A. Dubinin, D. Blaschke and A. Radzhabov, J. Phys. Conf. Ser. **668**, no. 1, 012052 (2016).